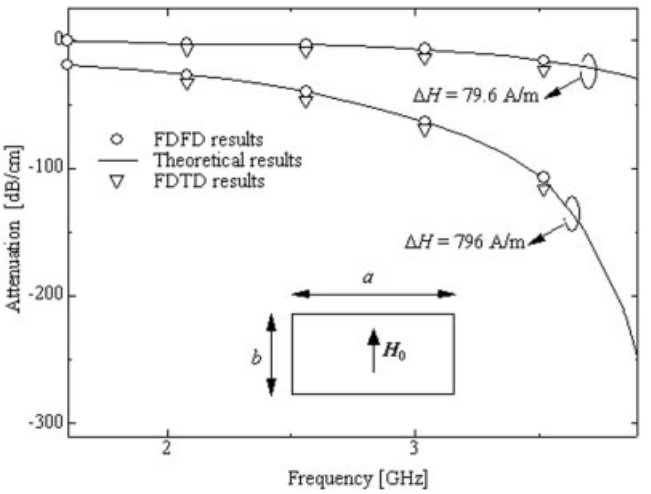

Figure 4 Numerical and theoretical results of the attenuation characteristics of a ferrite-filled waveguide: FDFD results (circles); theoretical results (lines); 3D FDTD results (triangles). a = 12.954 mm, b = 6.477 mm, $\mu_0 M_0$ = 178.0 mT, and $\mu_0 H_0$ = 80.0 mT

$$\omega_H = \gamma\mu_0(H_0 + j\Delta H/2), \tag{10}$$

$$\omega_M = \gamma\mu_0 M_0. \tag{11}$$

At first, the analysis is performed to obtain the dispersion characteristics of a ferrite-filled waveguide with $\mu_0 M_0$ = 178.0 mT, $\mu_0 H_0$ = 80.0, and 141.2 mT, respectively. The magnetic loss ΔH is assumed to be zero in this calculation. The numerical results calculated by the present method (see Fig. 3), agree very well with the theoretical results and the 3D FDTD numerical results. Secondly, the present method is also employed for analyzing the attenuation characteristic of a ferrite-filled waveguide. In this calculation, the magnetic losses ΔH are chosen as 79.6 and 796 A/m (1.0 and 10.0 Oe, respectively), $\mu_0 M_0$ = 178.0 mT, and $\mu_0 H_0$ = 141.2 mT. The results for these calculations, shown in Figure 4, also show good agreement with the theoretical results and the 3D FDTD numerical results.

4. CONCLUSION

A 2D FDFD method to analyze the dispersion characteristic of ferrite devices has been presented and demonstrated. The calculated result of the dispersion and attenuation characteristic of a ferrite-filled waveguide agrees very well with the theoretical result obtained from analytical approach and the 3D FDTD numerical result. Although the final eigen equation employed only four transverse-field components, it was confirmed to be sufficient for the analysis of the dispersion characteristics of ferrite devices. Therefore, it was shown to be more efficient than the method using six field components. In the calculation, although the elimination of longitudinal components does not help to reduce the memory-space requirement due to the increased number of terms in the remaining equations, the calculation time is considerably reduced, as compared to the case in which six field components are involved. Furthermore, when the frequency characteristic for a narrow range, for example, a resonator analysis made of artificial material, the FDFD method becomes more attractive, since it can effectively analyze the dispersion characteristics for a limited frequency range.

REFERENCES

1. J.A. Pereda, L.A. Vielva, A. Vegas, and A. Prieto, A treatment of magnetized ferrite using the FDTD method, IEEE Microwave Guided Wave Lett 3 (1993), 136–138.
2. A. Sanada, K. Okubo, and I. Awai, Full-wave finite-difference time-domain formulation for gyromagnetic ferrite media magnetized in arbitrary direction, IEICE Trans Electron E84-C (2001), 931–936.
3. J.A. Pereda, L.A. Vielva, M.A. Solano, A. Vegas, and A. Prieto, FDTD analysis of magnetized ferrites: Application to the calculation of dispersion characteristics of ferrite-loaded waveguides, IEEE Trans Microwave Theory Tech 43 (1995), 350–557.
4. E.O. Kamenetskii, A.K. Saha, and I. Awai, Effect of external circuit susceptance upon dual-mode coupling of a bandpass filter, Microwave Guided Wave Lett 10 (2000), 457–459.
5. I. Awai, H. Kubo, T. Iribe, and A. Sanada, Dielectric resonator based on artificial dielectrics and its application to a microwave BPF, Proc 32nd Euro Microwave Conf, 2002, pp 1045–1048.
6. R.E. Collin, Field theory of guided waves, 2nd ed., IEEE Press, New York, 1991, pp 749–786.

POLARIZATION-DEPENDENT ELECTROMAGNETIC BAND GAP (PDEBG) STRUCTURES: DESIGNS AND APPLICATIONS

Fan Yang and Yahya Rahmat-Samii
Electrical Engineering Department
University of California at Los Angeles
Los Angeles, CA 90095

Received 22 November 2003

ABSTRACT: *EBG structures exhibit an in-phase reflection coefficient, which makes them desirable for low-profile antenna designs. However, a conventional EBG structure has an identical reflection phase for a normally incident plane wave in spite of its polarization state. This paper presents novel polarization-dependent EBG (PDEBG) structures whose reflection phases are different, depending upon the polarization state of the incident plane wave. This polarization-dependent reflection-phase feature is realized by changing the unit geometries, for example, by using a rectangular patch to replace the square patch, by cutting slots into the patch, or by offsetting the vias. By properly tailoring the phase difference between different polarizations, a useful EBG reflector is introduced, which can control the polarization state of the reflected wave. One attractive application of this reflector is that the reflected wave of a circularly polarized incident plane wave can maintain its polarization sense.* © 2004 Wiley Periodicals, Inc. Microwave Opt Technol Lett 41: 439–444, 2004; Published online in Wiley InterScience (www.interscience.wiley.com).
DOI 10.1002/mop.20164

Key words: *anisotropic; electromagnetic band gap (EBG); polarization; reflector*

1. INTRODUCTION

Electromagnetic band-gap (EBG) structures have been widely explored in recent years [1–4]. They exhibit unique electromagnetic features, namely, the frequency band gap for surface waves and the in-phase reflection coefficient for incident plane waves. Various antenna and device applications have been proposed based on these features. For example, the in-phase reflection coefficient enables one to design low-profile wire antennas without losing radiation efficiency [5].

TABLE 1 Polarization States of Different Reflector Surfaces

Surface	Reflection Phase	Polarization of Incident Wave	Polarization of Reflected Wave
PEC	π	RHCP	LHCP
PMC	0	RHCP	LHCP
Traditional EBG	$\theta(f)$	RHCP	LHCP
PDEBG	$\theta(f, P)$	RHCP	RHCP, LP, elliptical polarization

This paper focuses on the reflection-phase feature of EBG structures. It is noted that a conventional EBG structure consisting of square unit cells has an identical reflection phase for a normally incident plane wave that is independent of its polarization state. Thus, it is an isotropic structure. Novel anisotropic EBG surfaces whose reflection phases are dependent on polarization states are investigated in this paper. Various polarization-dependent EBG (PDEBG) designs are presented, including a rectangular-patch EBG surface, a slot-loaded EBG surface, and an EBG surface with offset vias.

The applications of PDEBG surface are of special interest. In wireless communications, where low profile and polarization diversity are desired [6], the PDEBG surface can be used as a ground plane for a dipole antenna to generate circular polarization patterns or realize reconfigurable polarizations [7].

In this paper, the implementation of a PDEBG surface as a reflector is highlighted. It is well known that when a right-hand circularly polarized (RHCP) plane wave impinges onto a reflector using perfect electric conductor (PEC) with a reflection phase of 180°, the reflected plane wave becomes left-hand circularly polarized (LHCP), as illustrated in Table 1. The same thing happens for a PMC reflector whose reflection phase is zero. For a traditional EBG surfaces, the reflection phase θ is a function of frequency f but independent of polarization state P. Thus, the reflected plane wave is still LHCP. In contrast, the reflection phase of a PDEBG surface is dependent on both the frequency and polarization state. Therefore, when a PDEBG surface is used as a reflector, the polarization state of the reflected plane wave is determined by the reflection phase difference between two principal polarizations. When the phase difference is 180°, the reflected wave can maintain the RHCP. If the phase difference is 90°, the reflected wave will be linearly polarized (LP).

2. POLARIZATION-DEPENDENT EBG (PDEBG) SURFACE DESIGNS

This paper focuses on mushroomlike EBG structures which have compact unit sizes, as opposed to operational wavelength [2]. The finite-difference time-domain (FDTD) method is used to analyze the EBG surfaces [8]. To evaluate the reflection phase of the EBG surface, a plane wave is launched to normally illuminate the EBG surface. A single unit of the EBG surface with periodic boundary conditions (PBCs) on four sides is simulated to model an infinite surface. The perfectly matched layers (PML) are positioned a half-wavelength above the surface. The reflected plane wave from the EBG surface is recorded and the reflection phase is calculated accordingly. The phase-reference plane is located on the top of the EBG surface.

2.1. Rectangular-Patch EBG Surface

The traditional mushroomlike EBG structure uses square patch units so that its reflection phase for normal incidence is independent on the polarization of the incident plane wave. When square patches are replaced by rectangular patches, as shown in Figure 1(a), the reflection phase of the EBG surface is dependent on the X- or Y-polarization state of the incident plane wave. Figure 2(b) shows reflection phases of the rectangular-patch EBG surface, as compared to a square-patch EBG surface (the dimensions of the EBG surfaces are given in the caption of Fig. 1). When the incident plane wave is Y polarized, the rectangular-patch EBG surface has the same reflection phase as the square-patch EBG surface because the patch widths are the same. For the X-polarized incident plane wave, the patch length determines the reflection phase. Since the length is longer, the reflection phase shifts down to a lower frequency. It is noticed that near 3 GHz, the EBG surface shows a −90° reflection phase for the X-polarized wave and a 90° reflection phase for the Y-polarized wave. Thus, the phase difference between orthogonal polarizations is 180°.

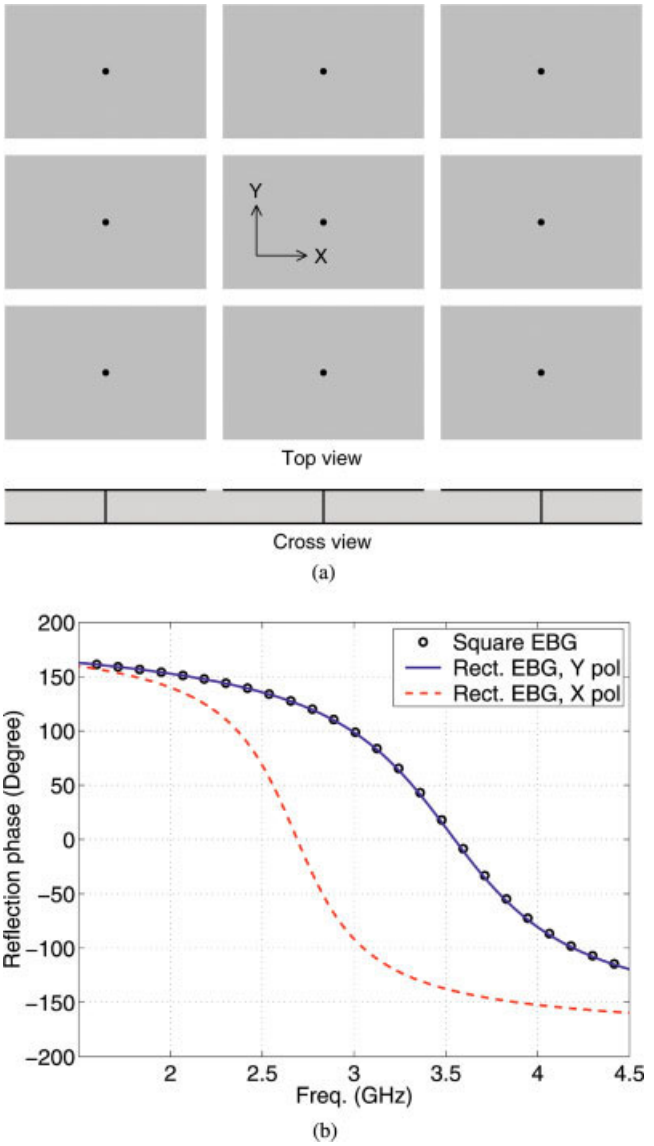

Figure 1 (a) A rectangular-patch EBG surface (0.24 λ_{3GHz} × 0.16 λ_{3GHz}) and (b) its reflection phases under different polarizations. A square-patch EBG surface (0.16 λ_{3GHz} × 0.16 λ_{3GHz}) is used as a reference. Gap width is 0.02 λ_{3GHz}, wire radius is 0.0025 λ_{3GHz}, substrate thickness is 0.04 λ_{3GHz}, and dielectric constant is 2.20. [Color figure can be viewed in the online issue, which is available at www.interscience.wiley.com.]

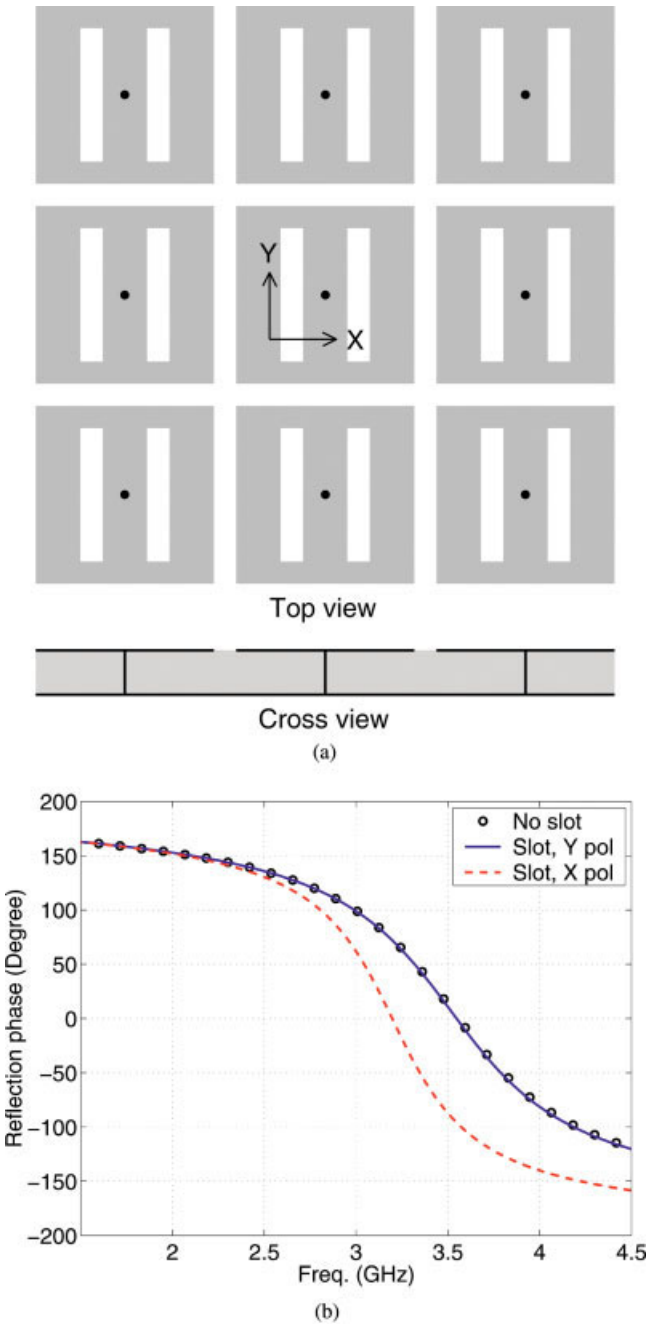

Figure 2 (a) A slot-loaded EBG surface and (b) its reflection phases under different polarizations. Two *Y*-oriented slots are symmetrically incorporated into the patch of a square EBG surface. [Color figure can be viewed in the online issue, which is available at www.interscience.wiley.com.]

2.2. *Slot-Loaded EBG Surface*

Another approach to realize polarization dependence is to cut slots into the patch. The advantage of this design is that one can obtain the same reflection-phase feature with a compact cell size. The operational mechanism exhibits an analogy similar to slot-loaded patch antennas. As shown in Figure 2(a), a pair of *Y*-oriented slots are symmetrically incorporated into the patch of a square EBG surface. The dimensions of the square-patch EBG are the same as those given in Figure 1. The slot length is 0.12 λ_{3GHz}, the slot width is 0.02 λ_{3GHz}, and the slot separation is 0.06 λ_{3GHz}. The slots affect electric currents flowing along the *X* direction, which results in a longer current path. Thus, the reflection phase of the *X*-polarized wave decreases to a low frequency, as depicted in Figure 2(b). In contrast, the reflection phase of the *Y*-polarized wave remains the same as the square-patch EBG surface because the slots have little effect on the electric currents flowing along the *Y* direction. The maximum reflection phase difference of this design is 98° obtained at 3.45 GHz.

2.3. *EBG Surface with Offset Vias*

Vias are critical components in a mushroomlike EBG structure. An EBG structure has two distinct electromagnetic features: the band gap of surface-wave propagation and the in-phase reflection coefficient; vias play different roles with respect to these two electromagnetic features. If the vias are removed, the band gap of surface wave will disappear [9]. In contrast, the reflection phase of a normally incident plane wave remains the same when the center vias are removed. The latter effect is similar to a center via in a microstrip patch antenna that does not affect the basic operating mode of the antenna. However, when the vias are offset from the center of the EBG patch, the reflection phase changes and the PDEBG surface can be realized.

As shown in Figure 3(a), the vias are offset along the *X* direction while they are still in the center along the *Y* direction. Therefore, the reflection phase for the *Y*-polarized wave remains unchanged and the reflection phase for the *X*-polarized wave changes with vias' position, as shown in Figure 3(b). When each via is in the center of the patch, only one resonance on the reflection phase is observed. Once the vias are offset, two resonances appear; one is higher than the original frequency and the other is lower. Different resonances correspond to the different widths of the left and right sides of the patch with respect to the vias. The left part is narrower and it forms the higher resonance. The right part is wider and resonates at a lower frequency. When the vias are closer to the patch edges, the separation of the two resonances increases because the width difference between two sides of the patch becomes longer.

To further understand this observation, an EBG surface with two symmetric vias under each patch is investigated, as shown in Figure 4(a). The distance between the vias and the patch edges is one-quarter of the patch width. Figure 4(b) compares the reflection-phase results of the single-via and double-vias cases. For the *Y*-polarized incident plane wave, they have the same reflection phase. When the incident plane wave is *X*-polarized, the double-via case shows only one resonance, which is very similar to the higher resonance of the single-via case. This observation verifies that the resonance feature is mainly determined by the distance between the vias and patch edges. For the single via case a 180° phase difference is achieved at 2.46 GHz, while for the double-via case the maximum phase difference of 96° is obtained at 3.77 GHz.

3. PDEBG APPLICATION: IN-POLARIZATION REFLECTOR

The polarization-dependent electromagnetic band gap (PDEBG) surface can be used as a reflector to realize special reflection function, namely, the in-polarization reflection. Figure 5 shows incident and reflected plane waves of a reflector as well as the coordinate system. To explain the polarization feature of the PDEBG reflector, we assume that the incident plane wave is right-hand circular polarized (RHCP) and normally illuminated upon the reflector as follows:

$$\vec{E}^i = \hat{x} \cdot e^{jkz} + \hat{y} \cdot j \cdot e^{jkz}. \quad (1)$$

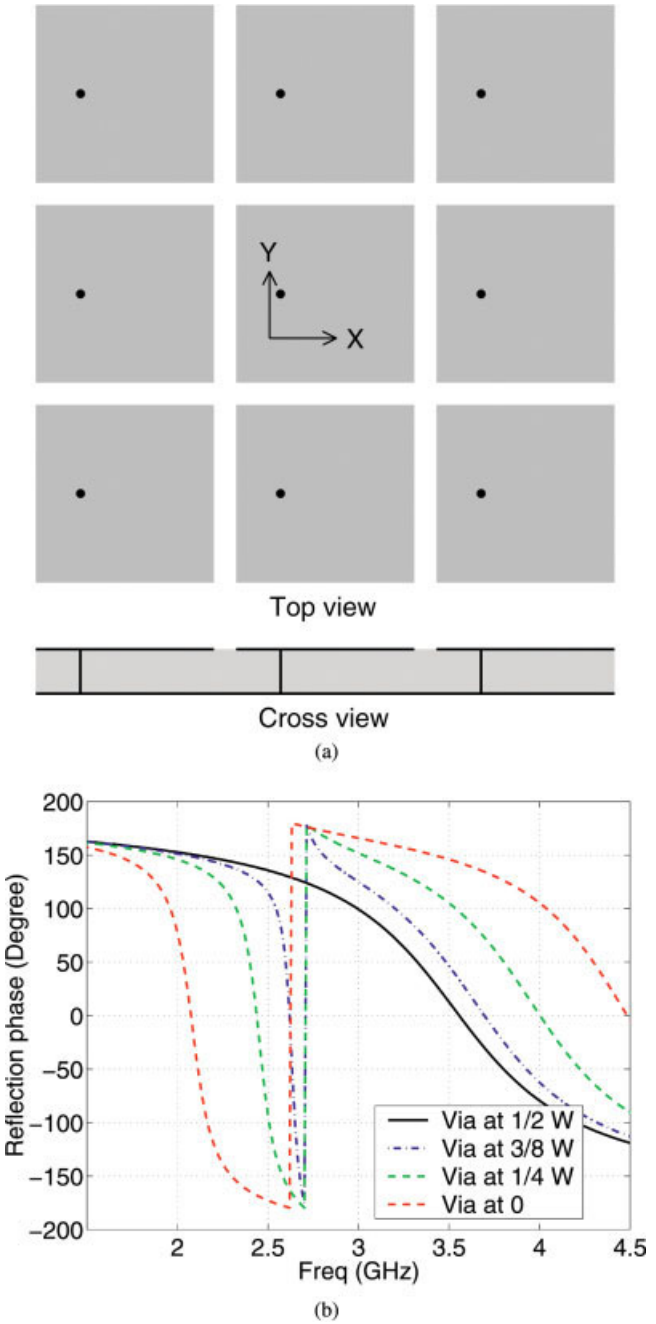

Figure 3 (a) An EBG surface with offset vias and (b) its reflection phases under different polarizations. [Color figure can be viewed in the online issue, which is available at www.interscience.wiley.com.]

The obtained reflected wave is given by

$$\vec{E}^r = \hat{x} \cdot e^{-jkz+j\theta_x} + \hat{y} \cdot j \cdot e^{-jkz+j\theta_y}, \tag{2}$$

where θ_x is the reflection phase for the X-polarized wave and θ_y is the reflection phase for the Y-polarized wave. Eq. (2) can be rewritten in terms of two circularly polarized components as

$$\vec{E}^r = e^{-jkz} \cdot e^{j\theta_x} \cdot \left[\hat{E}_L \cdot \left(\frac{1 + e^{j(\theta_y - \theta_x)}}{\sqrt{2}} \right) + \hat{E}_R \left(\frac{1 - e^{j(\theta_y - \theta_x)}}{\sqrt{2}} \right) \right], \tag{3}$$

$$\hat{E}_L = \frac{\hat{x} + \hat{y} \cdot j}{\sqrt{2}}, \tag{4}$$

$$\hat{E}_R = \frac{\hat{x} - \hat{y} \cdot j}{\sqrt{2}}, \tag{5}$$

where $\hat{E}_L$ is a unit vector that is left-hand circularly polarized (LHCP) and $\hat{E}_R$ is a unit vector that is right-hand circularly polarized (RHCP).

For a traditional reflector, such as the PEC reflector, $\theta_x = \theta_y$. Hence, the coefficient of the RHCP component is zero, and the reflected wave is purely LHCP. The same phenomenon happens for a PMC reflector or a conventional EBG surface whose reflection phase is independent of polarization states. Thus, the RHCP

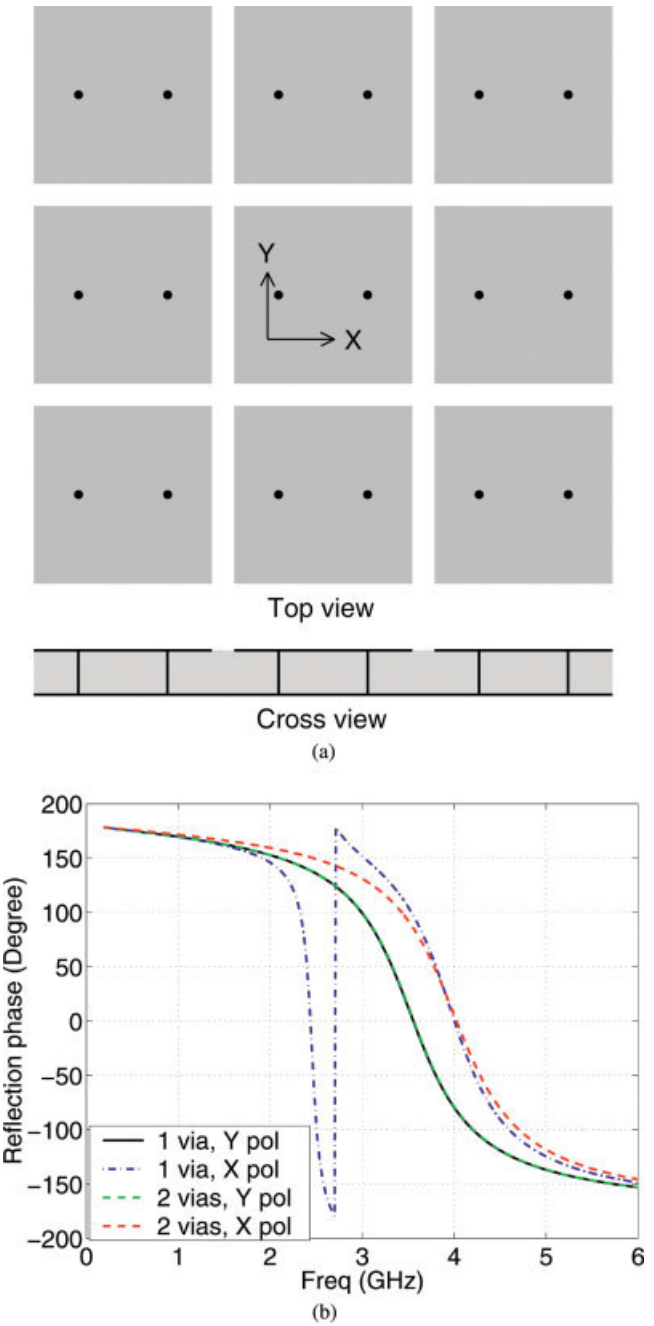

Figure 4 (a) An EBG surface with two symmetric offset vias under each patch and (b) its reflection phases under different polarizations. The distance between vias and patch edges is one-quarter of the patch width. [Color figure can be viewed in the online issue, which is available at www.interscience.wiley.com.]

plane wave changes to LHCP plane wave after reflection from these surfaces.

In order to realize in-polarization reflection, the polarization-dependent EBG surface is utilized as the reflector. The reflection phases of *X*- and *Y*-polarized waves are different, and their difference changes with frequency. At a certain frequency, the phase difference is 180°. Substituting this phase difference into Eq. (3), it can be found that the coefficient of the LHCP component becomes zero. As a result, the reflected wave remains RHCP.

To demonstrate this idea, the PDEBG surface designed in Figure 1 is used as an example. The phase difference ($\theta_y - \theta_x$) versus frequency is plotted in Figure 6(a). When the frequency is low, the phase difference is very small. The phase difference increases with the frequency increasing. When the frequency is 2.90 GHz, the phase difference is 180°. The phase difference reaches its maximum (193°) at 3.09 GHz and after that it decreases with frequency.

The axial ratio (AR) of the reflected wave is displayed in Figure 6(b). It is calculated from following equation [10]:

$$AR = -\frac{\|E_R\| + \|E_L\|}{\|E_R\| - \|E_L\|} = -\frac{\left\|\frac{1 - e^{j(\theta_y - \theta_x)}}{\sqrt{2}}\right\| + \left\|\frac{1 - e^{j(\theta_y - \theta_x)}}{\sqrt{2}}\right\|}{\left\|\frac{1 - e^{j(\theta_y - \theta_x)}}{\sqrt{2}}\right\| - \left\|\frac{1 - e^{j(\theta_y - \theta_x)}}{\sqrt{2}}\right\|}. \quad (6)$$

It is observed that, at 2.90 and 3.30 GHz, the axial ratio is equal to −1 and a purely RHCP-reflected wave is obtained. The frequency band inside which axial ratio of the RHCP reflected wave is below 3 dB ranges from 2.81 to 3.43 GHz (19.9%).

It is also noted that the reflected wave can be linearly polarized (LP) or LHCP, depending on the frequency and reflection phase difference. For example, at 2.58 GHz, the reflection phase difference is 90°. Thus, the reflected plane wave is linearly polarized with an axial ratio equal to infinity. The linear polarization direction is $\hat{x} + \hat{y}$, according to Eq. (3).

If one changes the roles of the incident and reflected waves, it can be inferred from Figure 6(b) that no matter what polarization of the incident wave is, the PDEBG reflector can change it to a purely RHCP plane wave by properly designing the phase difference of the surface.

4. CONCLUSION

This paper has presented several novel polarization-dependent electromagnetic band gap (PDEBG) structures. Three geometries to obtain polarization dependent reflection phase have been investigated, namely, rectangular-patch EBG, slot-loaded EBG, and EBG with offset vias. The reflection phases were simulated using the FDTD method, and the phase difference between the *X*- and *Y*-polarized plane waves was observed. Based on the phase difference, the PDEBG surface is utilized as a special reflector that exhibits interesting polarization behaviors. With a low-profile configuration, it can maintain the polarization sense of a circularly polarized plane wave after reflection, or change a linearly polarized incident wave to a circularly polarized reflected wave.

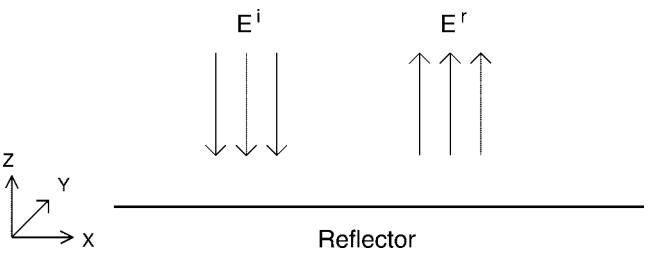

Figure 5 Incident and reflected plane waves of a reflector

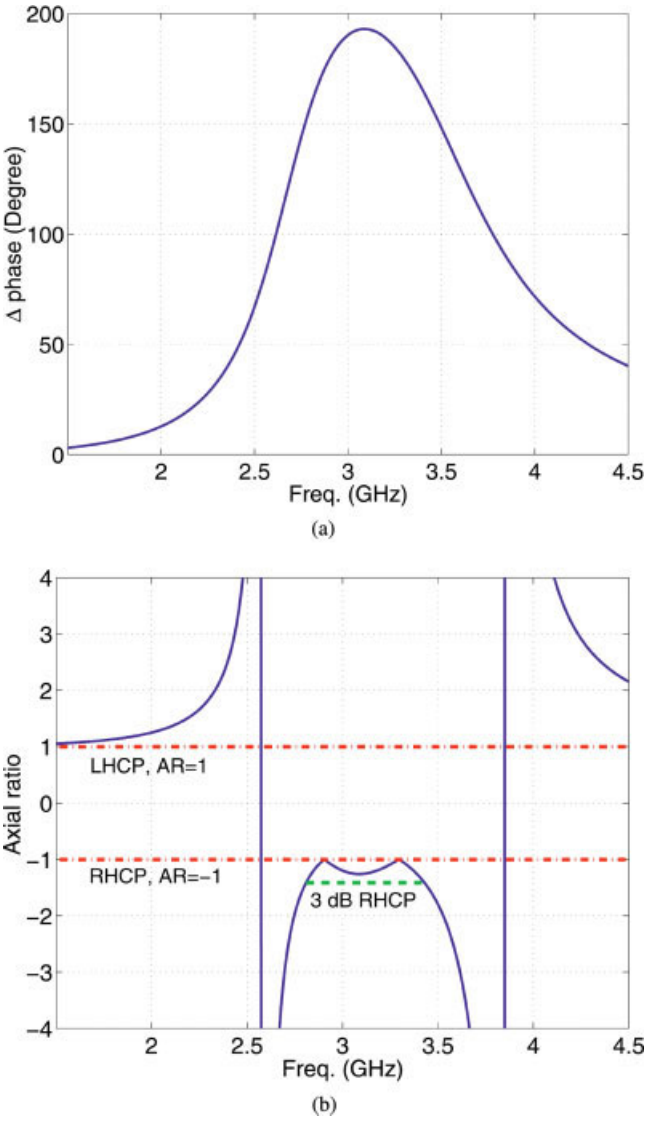

Figure 6 (a) Reflection-phase difference between different polarizations of the rectangular PDEBG surface shown in Fig. 1(a); (b) axial ratio of the reflected plane wave from the PDEBG reflector. [Color figure can be viewed in the online issue, which is available at www.interscience.wiley.com.]

REFERENCES

1. Y. Rahmat-Samii and H. Mosallaei, Electromagnetic band-gap structures: Classification, characterization, and applications, IEE-ICAP Symp 2001, pp. 560–564.
2. D. Sievenpiper, L. Zhang, R.F.J. Broas, N.G. Alexopolus, and E. Yablonovitch, High-impedance electromagnetic surfaces with a forbidden frequency band, IEEE Trans Microwave Theory Tech 47 (1999), 2059–2074.
3. A.S. Barlevy and Y. Rahmat-Samii, Characterization of electromagnetic band-gaps composed of multiple periodic tripods with interconnecting vias: Concept, analysis, and design, IEEE Trans Antennas Propagat 49 (2001), 242–353.
4. Special issue on meta-materials, IEEE Trans Antennas Propagat 51 (2003).
5. F. Yang and Y. Rahmat-Samii, Reflection phase characterizations of

the EBG ground plane for low profile wire antenna applications, IEEE Trans Antennas Propagat 51 (2003), 2691–2703.
6. W.E. Mckinzie III and R. Fahr, A low-profile polarization diversity antenna built on an artificial magnetic conductor, 2002 IEEE AP-S Int Symp Dig 1 (2002), 762–765.
7. F. Yang and Y. Rahmat-Samii, Polarization-dependent electromagnetic band-gap surfaces: characterization, designs, and applications, 2003 IEEE AP-S Dig 3 (2003), 339–342.
8. H. Mosallaei and Y. Rahmat-Samii, Broadband characterization of complex periodic EBG structures: an FDTD/Prony technique based on the split-field approach, Electromagn 23 (2003), 135–151.
9. A. Aminian, F. Yang, and Y. Rahmat-Samii, On the determination of the band gap region of EBG structures: a novel spectral FDTD approach, IEEE Trans Antennas Propagat (submitted).
10. C. Balanis, Advanced engineering electromagnetics, Wiley, New York, 1989.

NOVEL STRUCTURE OF AN ARRAYED-WAVEGUIDE GRATING MULTIPLEXER WITH FLAT SPECTRAL RESPONSE

Tsung-Hsin Lee,[1] Kun-Hung Tu,[1] and Ching-Ting Lee[2]
[1] Institute of Optical Sciences
National Central University
Chung-Li, 32054
Taiwan, Republic of China
[2] Institute of Microelectronics
Department of Electrical Engineering
National Cheng Kung University
Tainan, Taiwan, Republic of China

Received 18 November 2003

ABSTRACT: *A novel structure of arrayed-waveguide grating (AWG) multiplexers with a graded-index free-propagation region (FPR) used to increase the wavelength pass band is presented. The 1-dB and 3-dB wavelength pass bands increase with the increase of the graded-index FPR length. Flat and broadened spectral responses are obtained by using this novel structure.* © 2004 Wiley Periodicals, Inc. Microwave Opt Technol Lett 41: 444–445, 2004; Published online in Wiley InterScience (www.interscience.wiley.com). DOI 10.1002/mop.20165

Key words: *arrayed-waveguide grating; multiplexer; graded-index; FPR; PHASAR*

INTRODUCTION

Arrayed-waveguide grating (AWG) multiplexers are key components in optical dense wavelength-division multiplexing (DWDM) systems, because they process plural wavelengths simultaneously and they are capable of increasing the transmission capacity of single-strand optical fiber. The AWG multiplexer consists of input/output waveguides, two free-propagation regions (FPR), and a phased array (PHASAR) of multiple-channel waveguides with a constant optical-path-length difference between neighboring channel waveguides [1, 2]. When optical signals transmit through several filters in the DWDM ring/bus networks, flat and broadened spectral responses are required for the AWG multiplexer. In general, the optical output pattern of the input transmitter waveguide is a Gaussian distribution. To obtain uniform intensity for each of the output waveguides, the optical distribution propagating through FPR needs to be uniform. Furthermore, the optical phase needs to be changed. In previous reports [3–5], several methods to flatten the pass band of AWGs were proposed. In this study, we propose a novel flat-response AWG multiplexer using a graded-index FPR.

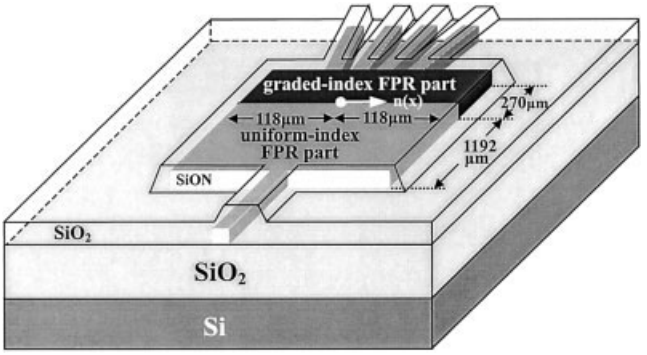

Figure 1 Configuration of the graded-index FPR of an AWG multiplexer

DESIGN AND RESULTS

Figure 1 shows the proposed graded-index FPR of an AWG multiplexer, which consists of one uniform-index FPR part and one graded-index FPR part. The refractive index of the uniform-index FPR part is the same as the channel waveguide. The refractive index in the center of the graded-index FPR part is the smallest, and it gradually increases with increasing distance from the center. The highest refractive index in the outer region of the graded-index FPR part is the same as the uniform-index FPR part. Since the higher refractive index in the outer region of the graded-index FPR part is designed, the Gaussian distribution of the optical field is redistributed into a uniform manner by the graded-index FPR part. Furthermore, the effectiveness of the graded-index FPR part can shift the focal point slightly. The phenomenon of this focal-point shift is similar to the function of using different path lengths in each arrayed waveguide of the AWG multiplexer [6]. The associated optical-intensity distribution on the boundary of the FPR and the output waveguides can be broadened.

In order to study performance of flattening by using the graded-index FPR, a 1×4 AWG multiplexer was designed, as shown in Figure 1. The length of the graded-index FPR part and the total length of this proposed graded-index FPR are 270 and 1462 μm, respectively. The refractive-index distribution $n(x)$ with regard to the width of the graded-index FPR part is designed as

$$n(x) = n_0 + (0.8 + 0.2x^2)\Delta n, \quad (1)$$

where $n_0 = 1.462$ is the refractive index of the SiO_2 cladding layer at a wavelength of 1.55 μm, and $\Delta n = 0.014$ is the refractive-index difference between the SiO_2 cladding layer and the silicon oxynitride channel waveguide. The width of this graded-index FPR is 336 μm. According to [7], the refractive index of silicon oxynitride film can be reduced by irradiating ultraviolet (UV) light. The UV-induced negative change depends on the UV-light density. By using a gray mask to control the irradiation UV light density, the required graded-index FPR part can be fabricated.

Figures 2(a) and 2(b) show the wavelength responses of the designed 1×4 AWG multiplexer without and with the graded-index FPR part, respectively. In order to compare the properties of the wavelength response for the wavelength peak of 1551.72 nm, the associated wavelength responses are shown in Figures 3(a) and 3(b), respectively. As shown in Figure 3(a) and 3(b), the flattened pass band can be obtained for the AWG multiplexer by the graded-index FPR part, where the 1-dB and 3-dB wavelength pass